Fabrication and improvement of nanopillar InGaN/GaN light-emitting diodes using nanosphere lithography

Fadil, Ahmed; Ou, Yiyu; Zhan, Teng; Wu, Kaiyu; Suyatin, Dmitry; Lu, Weifang; Petersen, Paul Michael; Liu, Zhiqiang; Ou, Haiyan

Published in:
Journal of Nanophotonics

DOI:
10.1117/1.JNP.9.093062

2015

Journal of Nanophotonics

Nanophotonics.SPIEDigitalLibrary.org

Fabrication and improvement of nanopillar InGaN/GaN light-emitting diodes using nanosphere lithography

Ahmed Fadil
Yiyu Ou
Teng Zhan
Kaiyu Wu
Dmitry Suyatin
Weifang Lu
Paul Michael Petersen
Zhiqiang Liu
Haiyan Ou

SPIE.

Fabrication and improvement of nanopillar InGaN/GaN light-emitting diodes using nanosphere lithography

Ahmed Fadil,[a,*] Yiyu Ou,[a] Teng Zhan,[b] Kaiyu Wu,[c] Dmitry Suyatin,[d] Weifang Lu,[a] Paul Michael Petersen,[a] Zhiqiang Liu,[b] and Haiyan Ou[a]

[a]Technical University of Denmark, DTU Fotonik, Ørsteds Plads 343, 2800 Kongens Lyngby, Denmark

[b]Chinese Academy of Sciences, Institute of Semiconductors, A35 Qinghua East Road, Haidian, Beijing 100083, China

[c]Technical University of Denmark, DTU Nanotech, Ørsteds Plads 345, 2800 Kongens Lyngby, Denmark

[d]Lund University, Division of Solid State Physics and The Nanometer Structure Consortium, Box 118, SE-22100 Lund, Sweden

Abstract. Surface-patterning technologies have enabled the improvement of currently existing light-emitting diodes (LEDs) and can be used to overcome the issue of low quantum efficiency of green GaN-based LEDs. We have applied nanosphere lithography to fabricate nanopillars on InGaN/GaN quantum-well LEDs. By etching through the active region, it is possible to improve both the light extraction efficiency and, in addition, the internal quantum efficiency through the effects of lattice strain relaxation. Nanopillars of different sizes are fabricated and analyzed using Raman spectroscopy. We have shown that nanopillar LEDs can be significantly improved by applying a combination of ion-damage curing techniques, including thermal and acidic treatment, and have analyzed their effects using x-ray photoelectron spectroscopy. [DOI: 10.1117/1.JNP.9.093062]

Keywords: light-emitting diodes; gallium nitride; nanopillar; damage treatment.

Paper 15026 received Apr. 15, 2015; accepted for publication Jul. 7, 2015; published online Aug. 7, 2015.

1 Introduction

The III-nitride-based light-emitting diodes (LEDs) have demonstrated very high efficiencies for blue emission wavelengths[1] and shown great potential for achieving energy efficiency for the entire visible spectrum. However, the internal quantum efficiency (IQE) suffers a significant decrease when moving toward emission wavelengths longer than blue.[2] Much effort has been made during last decade to improve the efficiency of InGaN-based LEDs through either the IQE or light extraction efficiency (LEE). Due to the high refractive index contrast between GaN and air, much of the light is trapped inside the LED epistructure; by employing surface texturing, the LEE can be improved. Surface roughening on the p-GaN surface has been investigated using chemical or laser etching to form roughness heights in the range of 5 to 20 nm, improving the wall-plug efficiency.[3,4] When nanostructures are fabricated on the n-GaN surface after removing the sapphire substrate, it is possible to achieve larger structures due to larger etch depths, and it has been reported that an output power increase by a factor of 2 to 3 could be obtained with feature sizes on the order of 500 nm.[5]

As opposed to random surface patterning, fabricating periodic and ordered nanostructures would allow a higher degree of control over the dimensions. Photonic crystal (PhC) structures are one example of nanopatterning that can improve light extraction by inhibiting lateral

*Address all correspondence to: Ahmed Fadil, E-mail: afad@fotonik.dtu.dk

1934-2608/2015/$25.00

propagation of light in the crystal and offer the possibility of modifying the IQE through the Purcell effect. PhC hole-pattern structure has been demonstrated on the p-GaN layer without penetrating the active region, showing improved output power.[6,7] PhC structure has also been investigated using a tunnel junction LED to enhance current spreading through the PhC region, with a resulting extraction efficiency improvement of factor 1.5.[8] For flip-chip LED design, the PhC structure needs to be formed on the n-GaN side, which has also been demonstrated.[9] The formation of nanostructures is not limited to the epilayers. Recently, attempts have been made to improve the device efficiency by fabricating PhC structures on a postgrowth deposition layer without modifying the epilayers, which avoids the disadvantage of active region damage from reactive-ion etching (RIE) processes.[10–12]

Simply etching the n-GaN or p-GaN layer to form nanostructures would not significantly modify the fabrication steps required to make ohmic contacts. There is, however, a greater potential for improved efficiency by etching through the active region to induce strain relaxation and weaken the quantum-confined Stark effect (QCSE).[13–22] Compared to blue, green InGaN quantum-well structures have a higher strain due to larger lattice mismatch as the InN mole fraction is increased.[23] The strain relaxation effects and the resulting IQE improvement are therefore expected to be higher for long-wavelength quantum-well emitters.

Fabricating nanostructures to induce strain relaxation can be achieved in several ways, including cost-effective techniques such as the use of self-assembled metal nanoparticles as etch mask[16–18] or nanosphere lithography (NSL).[19–22,24,25] The latter has the advantage of providing some degree of control over the periodicity and structure size in addition to the possibility of maximizing the active region fill factor. Early attempts at fabricating nanopillar structures using NSL with closely packed polystyrene (PS) nanospheres have employed metal templates formed in the interstices of the nanospheres, as etch mask.[24] Another approach is direct use of PS nanospheres as the masking material, whereby nanopillar structures can be formed through an RIE process and the pillar diameter can be varied by oxygen plasma etching of nanospheres.[25]

For InGaN/GaN LED epistructures, the effects of nanostructure size on strain relaxation and photoluminescence (PL) improvement have been investigated using periodic structures.[13–15] Various RIE damage-curing techniques have been tested including thermal annealing,[13] KOH to etch damaged side-walls,[15,18,21] and HCl treatment,[17,18] all exhibiting improved PL compared to as-etched samples.

In this work, we employ NSL in fabricating nanopillars on green LED epistructures, and Raman spectroscopy is used to confirm that strain relaxation takes place after nanopillar etching. We investigate two different post-etch damage curing techniques, i.e., rapid thermal annealing (RTA) and HCl chemical treatment, and how they can be combined to yield even greater improvement. We also consider how the treatments depend on nanopillar sizes.

2 Fabrication

The LED epitaxial structure was grown on a *c*-plane flat sapphire substrate by metal-organic chemical vapor deposition. Approximately 20-nm-thick low temperature GaN buffer layer was deposited followed by 2 μm u-GaN layer and 3 μm n-GaN:Si. Then, five periods of InGaN/GaN superlattice followed by five periods of InGaN/GaN multiple quantum-well (MQW) active region were grown. A 150 nm thick p-GaN:Mg and a 1 nm p-InGaN capping layer were then grown. For the NSL process, we deposited 150 nm SiO_2 by means of plasma-enhanced chemical vapor deposition. PS nanospheres with a diameter of 490 nm were used as templates for the patterning. To improve the hydrophilic properties of the substrate surface (top SiO_2 layer), the samples were exposed to oxygen plasma for 10 min. The PS nanosphere suspension consisted of 10% solids in aqueous solution (from Fisher Scientific ApS). The nanosphere suspension was then spin coated on the samples, applying several parameters.[26,27] We employed a two-step spin-coating process with a fast spin to spread the nanospheres, followed by a slow spin for drying. Our optimized parameters were a spin for 10 s at 2200 rpm with 600 rpm/s, followed by 30 s at 1000 rpm with 200 rpm/s. We used a drop of 10 μL on a 1×1 cm chip size. Using these parameters, a closely packed monolayer of PS nanospheres was obtained.

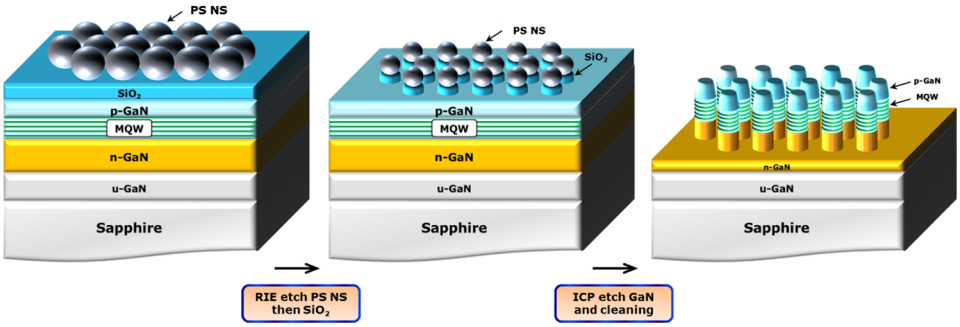

Fig. 1 Nanopillar fabrication process using nanosphere lithography. The SiO_2 layer is deposited prior to nanosphere (NS) spin-coating to serve as an etch mask for GaN etching. Reactive-ion etching (RIE) is used to shrink the NS size and form SiO_2 nanopillars, which is then transferred to GaN by an inductively coupled plasma (ICP)–RIE process. Acetone and hydrofluoric acid (HF) are used to remove the nanospheres and the SiO_2 layer.

To investigate different sizes of nanopillars, the PS nanospheres were shrunk to different sizes using oxygen plasma RIE, then an RIE process with CHF_3/N_2 chemistry at 50-W radio frequency (RF) power was used to etch the SiO_2. It is important that the plasma does not contain O_2 to avoid etching the PS nanospheres. Inductively coupled plasma (ICP) (RIE Plasmalab-100 system from Oxford Instruments) was then used to etch InGaN/GaN layers with Cl_2/Ar chemistry, where SiO_2 and the remaining PS nanospheres acted as etch mask. Process parameters were 400/75 W of ICP/RF power, 20/3 sccm flow rate of Cl_2/Ar, 5-mTorr process pressure, and 23° C platen temperature. Samples were etched for 3.5 min, and the obtained structure heights were in the range of 570 to 610 nm. After ICP etching, possible remnants of the PS nanospheres were cleaned using acetone followed by oxygen plasma etching. Subsequently, the SiO_2 layer was removed by 5% hydrofluoric acid (HF) wet etching. Damage-curing treatments, including RTA and HCl, were then applied at this step of the process. A schematic overview of the process is shown in Fig. 1.

3 Results and Discussions

The process of SiO_2 etching is not entirely harmless against the PS nanospheres. The selectivity of nanosphere diameter shrinking relative to SiO_2 etch-rate is approximately 1:3. This leads to SiO_2 nanopillars with angled side-walls, which are transferred to GaN nanopillars. As shown in the scanning electron microscope (SEM—Zeiss Supra V40 with 5 kV electron energy) images of Fig. 2, this effect is not severing due to the chosen thickness of SiO_2. It was not performed in this work, but if desired, a short KOH treatment can be applied to the InGaN/GaN nanopillars as anisotropic etching to produce vertical side-walls.[15] Four different samples were fabricated, each with a different nanopillar diameter. For three of the samples (A to C), the PS nanospheres were shrunk prior to SiO_2 etching, and for the fourth sample (D), the nanospheres remained as deposited and closely packed. As such, the different InGaN/GaN nanopillar top-surface diameters for samples A to D were 220, 360, 430, and 490 nm, respectively.

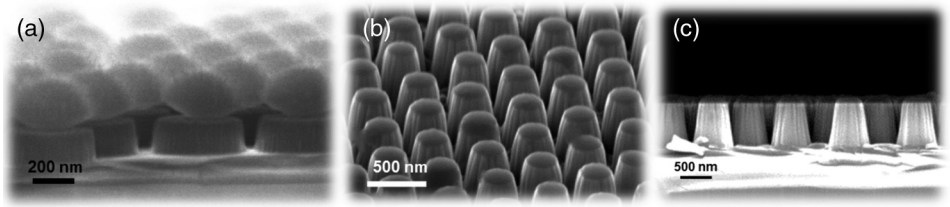

Fig. 2 Scanning electron microscopy (SEM) images showing (a) SiO_2 nanopillars with PS nanospheres. (b) Bird-eye view of the etched InGaN/GaN nanopillars and (c) the cross-sectional profile with remaining SiO_2 mask on top of the pillars.

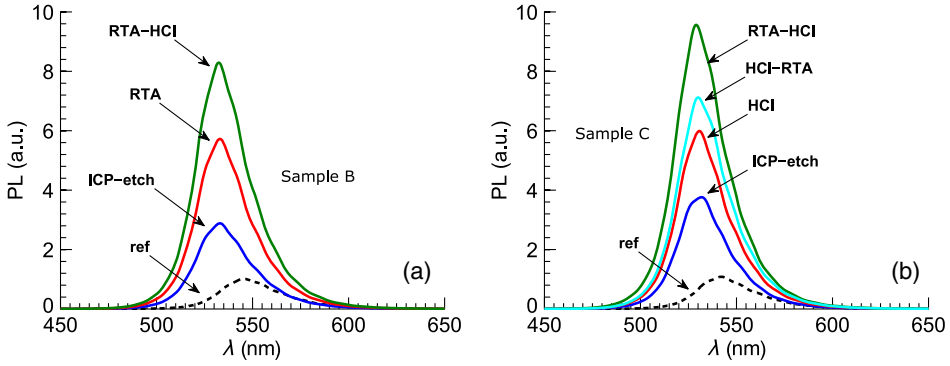

Fig. 3 (a) Photoluminescence (PL) spectra of sample B after formation of nanopillars (ICP-etch), after thermal annealing (RTA) and a combination of thermal annealing followed by 1-h HCl treatment. (b) The PL spectrum of sample C and the effects of different damage curing techniques.

After ICP etching and removal of SiO_2 together with PS nanospheres, PL measurements were conducted using a 405-nm excitation laser. The excitation and detection (using an Instruments Systems CAS 140CT Spectrometer) were from the sapphire side of the samples. The PL spectra of samples B and C are shown in Fig. 3, where all the intensities are normalized to the reference (as-grown) sample peak value. As mentioned previously, the ICP etching process of InGaN/GaN causes damage to the MQWs. To investigate the effects of different damage-curing techniques, we first performed RTA for 10 min at 500°C on sample B. The result is shown in Fig. 3(a), where PL intensity is enhanced compared to the as-etched nanopillar sample with an integrated PL enhancement ratio of 1.96. Succeeding the RTA process by a 1-h HCl treatment at room temperature further enhanced the PL. The combination of RTA-HCl treatment resulted in an enhancement by a factor of 2.82. On sample C, we first investigated the effect of HCl treatment alone, and the result was an enhancement by a factor of 1.57 relative to the as-etched sample. Following the HCl treatment by RTA did not show a significant improvement, as shown in Fig. 3(b). Apparently, the sequence of these damage-curing techniques is important when considering PL improvement and the combination provides a better result than either of them separately. This is witnessed by performing the RTA–HCl process on sample C and by observing a higher enhancement compared to the HCl–RTA case [Fig. 3(b)].

From the PL spectra of Fig. 3, it is noticed that the emission peak is blue-shifted compared to the as-grown sample, and this is an indication of strain relaxation. To further consolidate the strain relaxation effects, Raman spectra were measured using a Thermo Scientific Raman DXR microscope. The excitation laser wavelength was 780 nm focused to a spot size of 3.1 μm with 20 mW power. The Raman spectra of the samples are shown in Fig. 4. Considering the

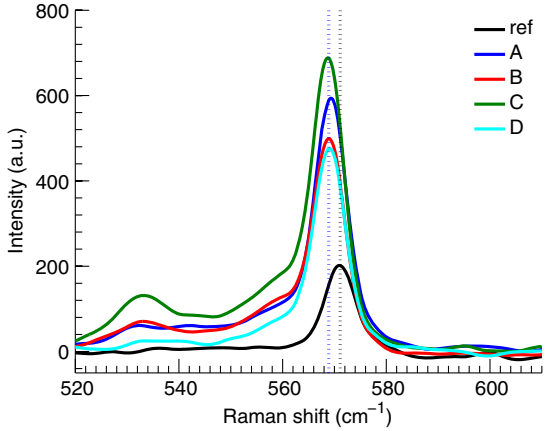

Fig. 4 Raman spectra of the samples A to D after nanopillar formation compared to the as-grown sample.

E_2 (high) phonon mode of GaN, we notice that the peaks of the etched samples are located around 569 cm^{-1}, whereas the reference sample has its E_2 (high) peak at 571 cm^{-1}. The E_2 phonon-mode peak shift toward lower energy affirms that strain relaxation has taken place in the InGaN/GaN MQWs.[22,28,29]

To further understand the effects of different treatments, we performed x-ray photoelectron spectroscopy (XPS) measurements using a Thermo K-Alpha system from Thermo Scientific with an Al K-Alpha source. The pass energy was set to 200.0 eV for the survey scan and 50.0 eV for high resolution scans. The reference peak energy is C 1*s*, C—C peak at 284.4 eV. A survey scan spectra is shown in Fig. 5(a). Comparing the as-etched sample spectrum with that of the reference, one difference to note is the F 1*s* peak at 685 eV, indicating the presence of fluorine contaminants, and is more clearly resolved in Fig. 5(b). Fluorine contaminants could have been introduced during the CHF_3-based RIE process, although their trace is eliminated either by thermal annealing or HCl treatment. Significant Cl 2*p* and Cl 2*s* peaks are present in the HCl-treated sample, as shown in Fig. 5(c). It appears that the Cl_2-based ICP–RIE etching of InGaN/GaN is not introducing similar levels of chlorine contaminants as the HCl treatment is. It has been known that HCl cleaning of GaN helps eliminate oxygen contaminants but leaves significant traces of chlorine, however the benefit of Cl is that it can tie up nitride dangling bonds and make the surface more resistant to reoxidization.[31] Since the as-grown sample has an InGaN capping layer, In $3d_{5/2}$ and In $3d_{3/2}$ core level peaks are measureable around binding energies of 444.8 and 452.2 eV, respectively, as seen from Fig. 5(d). The peak at 444.8 eV is likely due to indium native oxides (In_2O_3).[32] The two In 3*d* peaks vanish when the as-etched sample is cleaned in 5% HF to remove the SiO_2 mask. When the etched sample is exposed to air over a prolonged time, indium native oxides will be formed on the exposed surface of the InGaN well. It is, therefore, imperative that the nanopillar side-walls are protected, e.g., through a passivation layer. The thermal annealing and HCl treatments can also, by themselves, remove the native oxides (not shown). Figure 5(d) shows the combined effect of RTA–HCl treatment.

In Fig. 5(e), we consider the O 1*s* core level peak, which for the reference is deconvolved into three peaks at 530.4, 531.5, and 532.9 eV. For the as-etched sample, the lowest binding energy could not be resolved. The O 1*s* binding energy at 530.4 eV can be due to indium native oxides, In_2O_3.[32] The disappearance of this peak from the etched sample spectrum agrees with the findings from the In 3*d* spectra, where indium oxide has no trace for the as-etched sample. To understand why the peak disappears, we note that the as-etched sample has been treated with HF to remove SiO_2 mask. The HF treatment is expected to have etched away indium oxides, hence leaving no trace in the XPS spectra. The binding energy at 531.5 eV can be ascribed to chemisorbed oxygen atoms forming gallium oxides, Ga_2O_3, while the higher binding energy is likely due to O–H bonding from OH species.[31–35]

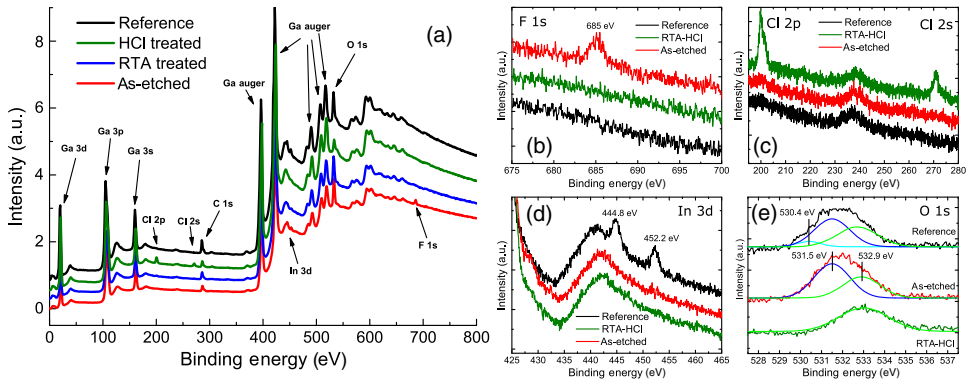

Fig. 5 (a) X-ray photoelectron spectroscopy spectra and highlights of notable differences between reference, etched, and surface-treated samples. The strong peaks near 400 eV are from Ga LMM Auger transitions.[30] (b) F 1*s* spectra, (c) Cl 2*p* and Cl 2*s* spectra and (d) In 3*d* spectra are shown for reference, etched and RTA–HCl treated samples. (e) O 1*s* spectra and peak deconvolution into three components for different samples. The as-etched spectra are shown after removing the SiO_2 masking layer using HF.

It is seen that the RTA–HCl treatment has left no trace of the 531.5 eV peak, indicating the removal of gallium oxides. The suppression of the O 1*s* peak was not achieved by the thermal annealing process alone, as happened to be case with the HCl treatment alone [Fig. 5(a)]. From these considerations, it would appear that HCl treatment outperforms thermal annealing, yet the combination of the treatments accomplishes a better result as witnessed by the PL emissions. An explanation could be that the wet chemical treatment of HCl only acts on the surface of the nanopillars, while RIE-induced damage and contaminants in the interior of the structures remain unaffected. Thermal annealing, on the other hand, will also affect the interior of the nanopillars and have the possibility of out-diffusing contaminants, and in this regard, it might have been advantageous to thermally anneal at higher temperatures.[13] This was not tested because we wanted to avoid annealing the samples at temperatures similar to or above the epilayer growth temperature. The combination of thermal annealing and HCl treatment is therefore expected to first cure interior damages and diffuse contaminants to the surface, while the HCl treatment thereafter cures the surface.

The damage-curing technique of thermal annealing followed by HCl treatment was then applied to samples A to D, and their PL spectra following this treatment are recorded in Fig. 6(a). Compared to the as-etched spectra, all samples demonstrate improved PL emission after the treatment. The integrated PL enhancements after nanopillar formation (post-ICP) and after the RTA–HCl treatment (total enhancement) are given in Table 1. The PL intensity is seen to increase from samples A to C, which is not a significant result considering that the active region fill factor increases from A to C due to diameter variations with a fixed pitch. By contrast, sample D with the largest fill factor demonstrates the lowest PL intensity peak. The inset of Fig. 6(a) shows a titled SEM view of sample D, where most nanopillars are seen to be connected to neighboring pillars. The connections can be expected to reduce the strain relaxation effects in the MQWs, and therefore, despite having the largest fill factor, the PL intensity of D is the weakest among the different samples.

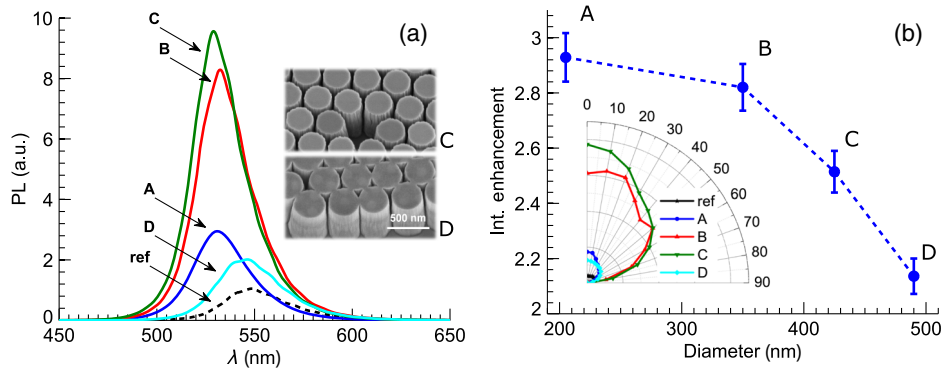

Fig. 6 (a) PL spectra of the samples after RTA–HCl treatment. Inset shows SEM images of samples C and D. (b) The integrated PL enhancements relative to the as-etched samples against nanopillar diameters. Inset is the angle-resolved PL for samples A to D.

Table 1 Sample characteristics and integrated photoluminance (PL) ratios.

Sample	NP-diameter (nm)	Emission CM blue shift (nm)	Post-ICP enhancement	RTA–HCl enhancement	Total enhancement
A	205	17.9	0.88	2.93	2.59
B	350	14.4	2.61	2.82	7.38
C	425	12.5	3.19	2.51	8.03
D	490	5.8	0.95	2.14	2.03

Note: ICP, inductively coupled plasma; RTA, rapid thermal annealing.

Blue shifts of the emission peaks are observed for all the etched samples relative to the reference indicating a reduced QCSE and strain relaxation. However, the amount of blue shift decreases with increasing nanopillar diameter (see Table 1), implying a higher strain relaxation with smaller nanopillar sizes, in agreement with earlier investigations.[14] We notice here that sample D demonstrates a smaller blue shift compared to the others (see Table 1), which gives another indication that strain relaxation effects are inhibited due to the connections between the nanopillars.

The enhancement due to RTA–HCl treatment (relative to as-etched samples) is shown in Fig. 6(b) for various sizes of nanopillars present in different samples. The included errorbars are estimated from a 2% uncertainty in the PL intensities. The total enhancement factors relative to the as-grown sample are listed in Table 1. Sample C demonstrated an integrated PL enhancement by a factor of 8, the highest among all the samples. However, we notice from Fig. 6(b) that the damage-curing treatment is more effective for smaller sized nanopillars. The enhancement for sample A with a pillar diameter of 205 nm is around a factor of 2.9, while that of the sample C is around 2.5. This trend could be due to more damage being introduced by the RIE processes when forming nanopillars of smaller diameter and thereby etching larger portions of the InGaN/GaN material. In such a scenario, the RTA–HCl treatment has a larger damage curing potential. However, since smaller nanopillars have a larger side-wall relative to the MQW area, another explanation could be that the HCl treatment has the possibility of reaching a larger surface area of the MQW side-walls relative to the MQW area on a single nanopillar. Larger nanopillars will have a smaller percentage of MQWs exposed from the side-walls of a single nanopillar, and therefore less damage can be cured by the HCl treatment.

The inset of Fig. 6(b) shows the far-field emission patterns. As a figure of merit (FOM) for the directionality, we estimate the percentage of power emitted inside a cone of 30 deg centered on the normal emission direction, which for the reference sample is 44%. The FOM for samples B and C are 59% and 60%, respectively, while sample A demonstrates the highest FOM of 65%. Not only did sample D show the weakest PL emission but also a poor directionality with a FOM of 55%. Small pillar sizes seem to be favorable when high directionality is desired.

4 Conclusion

We fabricated nanopillar structures on InGaN/GaN MQW LED using NSL and investigated the optical properties of different sized nanopillar structures. We could confirm that post-RIE damage treatment is critical for the optical performance of the LED, and in addition found that by combining two damage treatment methods, i.e., thermal annealing and HCl treatment, the PL improvement is better than either method applied separately. The order of these treatments is also of significance, with RTA–HCl resulting in a better performance than HCl–RTA. By using thermal annealing followed by HCl acidic treatment, an enhancement by a factor of 8 could be obtained relative to the as-grown sample. We also found that the RTA–HCl treatment was more effective for samples with smaller nanopillar diameters, i.e., when more of the active region had been etched away.

Acknowledgments

The authors would like to acknowledge the financial support by Innovation Fund Denmark Grant No. 0603-00494B, and the financial support provided by using the Lund Nano Lab Facilities which is financed by the Nanometer Structure Consortium.

References

1. Y. Narukawa et al., "Improvement of luminous efficiency in white light emitting diodes by reducing a forward-bias voltage," *Jpn. J. Appl. Phys.* **46**(40), L963–L965 (2007).
2. T. Takeuchi et al., "Quantum-confined Stark effect due to piezoelectric fields in GaInN strained quantum wells," *Jpn. J. Appl. Phys.* **382**, L382 (1997).
3. C. Huh et al., "Improved light-output and electrical performance of InGaN-based light-emitting diode by microroughening of the p-GaN surface," *J. Appl. Phys.* **93**(11), 9383 (2003).

4. H.-W. Huang et al., "Enhanced light output of an InGaN/GaN light emitting diode with a nano-roughened p-GaN surface," *Nanotechnology* **16**(9), 1844–1848 (2005).
5. T. Fujii et al., "Increase in the extraction efficiency of GaN-based light-emitting diodes via surface roughening," *Appl. Phys. Lett.* **84**(6), 855 (2004).
6. T. N. Oder et al., "III-nitride blue and ultraviolet photonic crystal light emitting diodes," *Appl. Phys. Lett.* **84**(2004), 466–468 (2004).
7. S. H. Kim et al., "Fabrication of photonic crystal structures on light emitting diodes by nanoimprint lithography," *Nanotechnology* **18**(5), 055306 (2007).
8. J. J. Wierer et al., "InGaN/GaN quantum-well heterostructure light-emitting diodes employing photonic crystal structures," *Appl. Phys. Lett.* **84**(19), 3885 (2004).
9. J. J. Wierer, A. David, and M. M. Megens, "III-nitride photonics-crystal light-emitting diodes with high extraction efficiency," *Nat. Photonics* **3**, 163–169 (2009).
10. T. Truong et al., "Light extraction from GaN-based light emitting diode structures with a noninvasive two-dimensional photonic crystal," *Appl. Phys. Lett.* **94**(2), 023101 (2009).
11. K. Byeon et al., "Fabrication of SiN x-based photonic crystals on GaN-based LED devices with patterned sapphire substrate by nanoimprint lithography," *Opt. Express* **20**(10), 11423–11432 (2012).
12. K. H. Li and H. W. Choi, "InGaN light-emitting diodes with indium-tin-oxide photonic crystal current-spreading layer," *J. Appl. Phys.* **110**(5), 053104 (2011).
13. S. Keller et al., "Optical properties of GaN nanopillar and nanostripe arrays with embedded InGaN/GaN multi-quantum wells," *J. Appl. Phys.* **100**, 054314 (2006).
14. V. Ramesh et al., "Strain relaxation effect by nanotexturing InGaN/GaN multiple quantum well," *J. Appl. Phys.* **107**, 114303 (2010).
15. S. Bae et al., "Size-controlled InGaN / GaN nanorod array fabrication and optical characterization," *Opt. Express* **21**(14), 16854 (2013).
16. Q. Wang et al., "Influence of strain relaxation on the optical properties of InGaN/GaN multiple quantum well nanorods," *J. Phys. D: Appl. Phys.* **44**(39), 395102 (2011).
17. J. Zhu et al., "Light extraction efficiency improvement and strain relaxation in InGaN/GaN multiple quantum well nanopillars," *J. Appl. Phys.* **109**, 1–6 (2011).
18. J. De-Sheng and W. Hai, "Fabrication and optical characterization of GaN-based nanopillar light emitting diodes," *Chin. Phys. Lett.* **3485**(9), 3485 (2008).
19. L.-Y. Chen et al., "High performance InGaN/GaN nanorod light emitting diode arrays fabricated by nanosphere lithography and chemical mechanical polishing processes," *Opt. Express* **18**(8), 7664–7669 (2010).
20. K. H. Li and H. W. Choi, "Air-spaced GaN nanopillar photonic band gap structures patterned by nanosphere lithography," *J. Appl. Phys.* **109**(2), 023107 (2011).
21. Q. Li et al., "Optical performance of top-down fabricated InGaN/GaN nanorod light emitting diode arrays," *Opt. Express* **19**(25), 25528–25534 (2011).
22. P. Dong et al., "Optical properties of nanopillar AlGaN/GaN MQWs for ultraviolet light-emitting diodes," *Opt. Express* **22**(S2), A320 (2014).
23. T. Takeuchi et al., "Quantum-confined Stark effect due to piezoelectric fields in GaInN strained quantum wells," *Jpn. J. Appl. Phys.* **382**, L382 (1997).
24. C.-W. Kuo et al., "Fabrication of size-tunable large-area periodic silicon nanopillar arrays with sub-10-nm resolution," *J. Phys. Chem. B* **107**(37), 9950–9953 (2003).
25. C. L. Cheung et al., "Fabrication of nanopillars by nanosphere lithography," *Nanotechnology* **1339**, 1339–1343 (2006).
26. J. Chen et al., "Controllable fabrication of 2D colloidal-crystal films with polystyrene nanospheres of various diameters by spin-coating," *Appl. Surf. Sci.* **270**, 6–15 (2013).
27. P. Colson, R. Cloots, and C. Henrist, "Experimental design applied to spin coating of 2D colloidal crystal masks: a relevant method?," *Langmuir* **27**(21), 12800–12806 (2011).
28. T. Sugiura et al., "Raman scattering study of InGaN grown by metalorganic vapor phase epitaxy on (0001) sapphire substrates," *Jpn. J. Appl. Phys.* **40**, 5955–5958 (2001).
29. P. Puech et al., "GaN nanoindentation: a micro-Raman spectroscopy study of local strain fields," *J. Appl. Phys.* **96**, 2853–2856 (2004).
30. J. B. Metson et al., "X-ray absorption spectroscopy in the analysis of GaN thin films," *Surf. Interface Anal.* **35**(9), 719–722 (2003).

31. S. W. King et al., "Cleaning of AlN and GaN surfaces," *J. Appl. Phys.* **84**(9), 5248–5260 (1998).
32. J. F. Moulder et al., *Handbook of Photoelectron X-ray Spectroscopy*, J. Chastain, Ed., Eden Prairie, Minnesota (1992).
33. K. Prabhakaran, T. G. Andersson, and K. Nozawa, "Nature of native oxide on GaN surface and its reaction with Al," *Appl. Phys. Lett.* **69**, 3212 (1996).
34. D. Li et al., "Selective etching of GaN polar surface in potassium hydroxide solution studied by x-ray photoelectron spectroscopy," *J. Appl. Phys.* **90**(8), 4219–4223 (2001).
35. M. Mishra et al., "Pits assisted oxygen chemisorption on GaN surfaces," *Phys. Chem. Chem. Phys.* **17**, 15201–15208 (2015).

Biographies of the authors are not available.